View metadata, citation and similar papers at core.ac.uk
brought to you by CORE
provided by DSpace@MIT

A Description of Local and Nonlocal Eddy–Mean Flow Interaction in a Global Eddy-Permitting State Estimate

RU CHEN

Scripps Institution of Oceanography, University of California, San Diego, La Jolla, California

GLENN R. FLIERL

Massachusetts Institute of Technology, Cambridge, Massachusetts

CARL WUNSCH

Massachusetts Institute of Technology, and Harvard University, Cambridge, Massachusetts

(Manuscript received 3 January 2014, in final form 6 May 2014)

ABSTRACT

The assumption that local baroclinic instability dominates eddy–mean flow interactions is tested on a global scale using a dynamically consistent eddy-permitting state estimate. Interactions are divided into local and nonlocal. If all the energy released from the mean flow through eddy–mean flow interaction is used to support eddy growth in the same region, or if all the energy released from eddies through eddy–mean flow interaction is used to feed back to the mean flow in the same region, eddy–mean flow interaction is local; otherwise, it is nonlocal. Different regions have different characters: in the subtropical region studied in detail, interactions are dominantly local. In the Southern Ocean and Kuroshio and Gulf Stream Extension regions, they are mainly nonlocal. Geographical variability of dominant eddy–eddy and eddy–mean flow processes is a dominant factor in understanding ocean energetics.

1. Introduction

The ocean circulation is generated as a result of the external forces including winds, tides, and heat exchanges with the atmosphere (e.g., Huang 2004; Ferrari and Wunsch 2010). Several studies have described the spatiotemporal patterns of the wind work and have estimated that the total wind power input into the surface geostrophic flow in the global ocean is roughly 0.8 TW (e.g., Wunsch 1998; Scott and Xu 2009). However, the uncertainty of this number is large (Zhai et al. 2012). The ways in which the energy, momentum, vorticity, and enstrophy from these external forces move through the global ocean, transform in their nature and scale, are exchanged with the atmosphere and cryosphere, and are dissipated are extremely complicated. Many aspects of this process are still unknown and full descriptions do not exist.

The ocean circulation varies on a broad range of spatiotemporal scales, and the time-varying flows can exchange energy, vorticity, and momentum with the time-mean circulation through eddy–mean flow interaction. These exchanges influence the nature of both the mean and the perturbations. Within the ocean, the time-mean circulation contains most of the potential energy, whereas the time-varying flow contains most of the kinetic energy. A large body of literature exists on the conversion of energy from the time-mean circulation to the time-varying flow through barotropic, baroclinic, mixed instability processes, etc. (e.g., Gill et al. 1974; Pedlosky 1987; Spall 2000; Vallis 2006). Energy from the time-varying flow can also be transferred back to the time-mean circulation through a variety of processes including rectification and topographic steering (e.g., Whitehead 1975; McWilliams et al. 1978; Marshall 1984; Johnson et al. 1992; Witter and Chelton 1998); similar phenomena are found in atmospheric jet streams (e.g., Williams et al. 2007). At the same time, energy can also be redistributed among different spatial scales/vertical modes through energy cascades (e.g., Salmon 1978;

Corresponding author address: Ru Chen, Scripps Institution of Oceanography, University of California, San Diego, 8622 Kennel Way, La Jolla, CA 92037.
E-mail: ruchen@alum.mit.edu

DOI: 10.1175/JPO-D-14-0009.1

© 2014 American Meteorological Society

Fu and Flierl 1980; Scott and Wang 2005) and be transmitted over large distances through, for example, advection or the propagation of rings and waves.

Von Storch et al. (2012) studied the ocean Lorenz energy cycle using a 0.1° global simulation and suggested that even though eddy–mean flow interaction in the ocean involves many physical processes, the dominant globally integrated energy pathway between eddies and the mean flow in both the ocean and the atmosphere is identical to the energy pathway in idealized local baroclinic instability processes (Lorenz 1955; Pedlosky 1987). In the global ocean, the generation rate of eddy kinetic energy through this energy pathway is roughly one-third of the total wind power input into the geostrophic flow (Ferrari and Wunsch 2009; Scott and Xu 2009).

A large literature exists discussing the simple and yet compelling *local baroclinic instability hypothesis*, its plausibility in the midocean, and its utility in explaining eddy properties and generation in the global ocean (e.g., Robinson and McWilliams 1974; Held and Larichev 1996; Venaille et al. 2011; Smith 2007; Tulloch et al. 2011). This hypothesis has two aspects: 1) each region in the ocean is assumed to be horizontally homogeneous, and thus all the energy released from the baroclinically unstable mean flow is used to sustain the local eddy energy growth, which is balanced by other terms in the eddy energy budget (e.g., mixing and dissipation); and 2) the dominant source for eddy growth in this patch is the energy released from the mean flow through baroclinic instability, not from advection, external forcing, etc. (e.g., Tulloch et al. 2011). Observed eddies in the midocean have similar properties to those from local linear baroclinic instability analysis and to those from relevant idealized experiments with reasonable parameters, indicating the plausibility of this hypothesis in the midocean (Gill et al. 1974; Arbic and Flierl 2004). Motivated by this, many oceanic problems (e.g., jet dynamics, eddy heat fluxes, time-dependent instabilities, and energy cascades) have been investigated in the doubly periodic two-layer model with vertical shear in which local baroclinic instability occurs (e.g., Salmon 1978; Panetta 1993; Thompson 2010).

This study is concerned with the first aspect of the local baroclinic instability hypothesis, which is assumed in many instability theories (Pedlosky 1987). The actual time-mean circulation is not homogeneous (Arbic 2000; Tulloch et al. 2011), implying that the energy released from the mean flow through eddy–mean flow interaction can be transmitted to other regions through the divergence term (Kundu and Cohen 2004; Liang and Robinson 2007). The amount of energy transmitted elsewhere and the impact of this nonlocal nature of eddy–mean flow interaction on energy cascades, eddy fluxes, jet dynamics, and eddy properties are still largely unknown.

The goals of this mainly descriptive paper are simply to 1) map the respective change rate of energy in eddies and the mean flow through eddy–mean flow interaction and 2) characterize the regional energy route through eddy–mean flow interaction and discuss whether the energy released from the mean flow is used to support the local eddy energy growth in energetic regions. The oceanic community lacks the long-term observations of global velocity, salinity, and density fields, which are needed to pursue this study. Until such time as useful observations become available, diagnostics from models are a useful way to explore energy movement (e.g., Cox 1987; von Storch et al. 2012; Zhai and Marshall 2013). Here we use an eddying global simulation [i.e., the Estimating the Circulation and Climate of the Ocean, phase 2, high-resolution global-ocean and sea ice data synthesis (ECCO2) state estimate], noting that it is dynamically consistent and thus applicable to the energy budget analysis and assuming that the simulated oceanic circulation is quantitatively accurate enough for the task (Chen 2013). We present the diagnostic framework in section 2, the configuration and fidelity of the ECCO2 state estimate in section 3, the key results about eddy–mean flow interaction in section 4, and the summary in section 5.

2. Diagnostic framework

a. *Definition of kinetic energy and available potential energy*

Oceanic variability encompasses a continuum of spatial scales, ranging from submesoscale and mesoscale motions to gyre shifts and basin oscillations; it also spans a wide range of temporal scales, ranging from superinertial to seasonal and decadal variability. In this study, mean flow refers to the flow temporally averaged over the specific 16 yr (1992–2007) available from the ECCO2 state estimate. The entire time-varying flow in the ECCO2 state estimate, which is the deviation from the 16-yr average and independent of spatial scale, is termed ''eddies'' as a short hand. One caveat is that decadal variability and submesoscale variability at a horizontal scale of a few kilometers, though not resolved in the ECCO2 state estimate, might contribute significantly to the energy budget. Also note that eddies at different spatiotemporal scales probably contribute differently to the eddy–mean flow interaction, though we do not consider this issue here.

The kinetic energy in the mean flow (MKE) is defined as

$$K_M(x,y,z) = 0.5\rho_0(\overline{u}^2 + \overline{v}^2), \tag{1}$$

and the kinetic energy in the time-varying flow (EKE) is defined as

$$K_E(x,y,z) = 0.5\rho_0\overline{(u'^2 + v'^2)}, \tag{2}$$

where u is zonal velocity, v is meridional velocity, the overbar hereafter denotes the time mean, and the prime denotes the deviation from the time mean. The term ρ_0 is the constant reference density (1027.5 kg m^{-3} in the ECCO2 state estimate).

Available potential energy (APE) refers to the difference in potential energy between the actual state (i.e., the oceanic state in the ECCO2 state estimate) and a reference state where the potential energy is minimal under adiabatic and mass-conserving rearrangement of the fluid (Margules 1905; Lorenz 1955; Oort et al. 1989; Huang 2005). Several forms of APE exist (Huang 2005; Tailleux 2013) and we choose one that is analogous to the quasigeostrophic definition widely used (e.g., Pedlosky 1987; Oort et al. 1989, 1994; Huang 2010; Brown and Fedorov 2010):

$$P(x,y,z) = -\frac{g}{2n_0}\overline{\rho^*(x,y,z,t)^2}, \tag{3}$$

where $\rho^*(x, y, z, t) = \rho(x, y, z, t) - \langle\overline{\rho(x, y, z, t)}\rangle$, and $\langle\cdot\rangle$ denotes the global mean at a given depth. The variable n_0 is the time and global mean of the vertical gradient of local potential density, that is,

$$n_0(z) = -\frac{\rho_0}{g}N^2(z) = \left\langle\overline{\left[\frac{\partial\rho(x,y,z,t)}{\partial z}\right]}_{x,y,t}\right\rangle - \left\langle\overline{\left[\frac{\partial\rho(S,\theta,z)}{\partial z}\right]}_{S,\theta}\right\rangle, \tag{4}$$

where $N^2(z)$ is the time and global mean of the buoyancy frequency (Huang 2010), and S and θ denote salinity and potential temperature, which are functions of space and time. The terms $\rho(x, y, z, t)$, $\overline{\rho(x, y, z, t)}$, and $\langle\overline{\rho(x, y, z, t)}\rangle$ are the in situ density in the instantaneous actual state, in the time-mean actual state, and in the reference state, respectively. Mean available potential energy (MAPE) is the difference between the potential energy stored in the time-mean actual state and that in the reference state, that is,

$$P_M(x,y,z) = -\frac{g}{2n_0}\overline{\rho^*(x,y,z,t)}^2. \tag{5}$$

Eddy available potential energy (EAPE) is the difference between the potential energy in the instantaneous actual state and that in the time-mean actual state, that is,

$$P_E(x,y,z) = -\frac{g}{2n_0}\overline{\rho'(x,y,z,t)^2}. \tag{6}$$

Note that $P(x, y, z) = P_M(x, y, z) + P_E(x, y, z)$. Equations (5) and (6) have recently been used to evaluate the Lorenz energy cycle in the global ocean and the energy budget of time-varying flows with periods from 10 min to 10 yr (von Storch et al. 2012). The form of Eq. (3) may not accurately represent the true amount of APE, but it gives a local estimate while preserving the transfers from kinetic energy: the diagnostic framework [Eqs. (7)–(10)], based on the energy definitions above, is mathematically self-consistent and is useful for evaluating the eddy–mean flow interaction problem.

b. Energy equations for the mean flow and eddies

In some atmospheric and Southern Ocean studies, mean flow is often defined as the zonal average, and the transformed Eulerian mean framework is used to explore eddy–mean flow interaction (e.g., Plumb and Ferrari 2005; Kuo et al. 2005; Vallis 2006). Here we need a framework consistent with our definition of eddies and mean flow. A detailed derivation of the kinetic and available potential energy equations consistent with the ECCO2 state estimate is provided in the appendix. These equations are

$$\frac{\partial}{\partial t}K_M + \nabla\cdot(\overline{\mathbf{u}}K_M) + \nabla\cdot(\overline{\mathbf{u}}\overline{p^*}) = -D_{K_M} + M_{K_M} + X_{K_M}, \tag{7}$$

$$\frac{\partial}{\partial t}K_E + \nabla\cdot\overline{[\mathbf{u}\rho_0(u'^2 + v'^2)/2]} + \nabla\cdot\overline{(\mathbf{u}'p')} = D_{K_E} + M_{K_E} + X_{K_E}, \tag{8}$$

$$\frac{\partial}{\partial t}P_M + \nabla\cdot(\overline{\mathbf{u}}P_M) = D_{P_M} + D_{K_M} + X_{P_M} + R_{P_M}, \quad \text{and} \tag{9}$$

$$\frac{\partial}{\partial t}P_E + \nabla\cdot\overline{[-\mathbf{u}g\rho'^2/(2n_0)]} = D_{P_E} - D_{K_E} + X_{P_E} + R_{P_E}, \tag{10}$$

where $\mathbf{u}$ is the three-dimensional velocity vector, ∇ is the three-dimensional gradient operator, p is the hydrostatic pressure, and $p^*(x, y, z, t) = p(x, y, z, t) - \langle\overline{p(x, y, z, t)}\rangle$. Note that

$$\frac{\partial}{\partial z}p^* = -\rho^* g, \quad \frac{\partial}{\partial z}p' = -\rho' g. \tag{11}$$

TABLE 1. The eddy–mean flow interaction terms on which this study focuses. The term $\mathbf{u}_H$ is the horizontal velocity vector, and ∇_H is the horizontal gradient operator.

Term	Mathematical form	Meaning
D_{P_M}	$\frac{g}{n_0}\overline{\rho^*}\nabla_H\cdot(\overline{\mathbf{u}'_H\rho'})$	MAPE change rate due to horizontal eddy density fluxes.
D_{P_E}	$\frac{g}{n_0}\overline{\mathbf{u}'_H\rho'}\cdot\nabla_H\overline{\rho^*}$	Eddy energy (EAPE + EKE) change rate due to horizontal eddy density fluxes.
D_{K_E}	$-g\overline{\rho' w'}$	Gain rate of EKE from EAPE.
M_{K_M}	$-\rho_0[\overline{u}\nabla\cdot(\overline{u'\mathbf{u}'})+\overline{v}\nabla\cdot(\overline{v'\mathbf{u}'})]$	MKE change rate due to eddy momentum fluxes.
M_{K_E}	$-\rho_0(\overline{u'\mathbf{u}'}\cdot\nabla\overline{u}+\overline{v'\mathbf{u}'}\cdot\nabla\overline{v})$	EKE change rate due to eddy momentum fluxes.

The terms on the left-hand side of Eqs. (7)–(10) represent the temporal change rates of energy and the redistribution rates of energy through advection and pressure work. The temporal change rates are negligible in the energy budgets. Considering the goal of this study, we focus on the eddy–mean flow interaction terms listed in Table 1: the D terms are eddy–mean flow interaction terms related to eddy density fluxes, and the M terms are eddy–mean flow interaction terms related to eddy momentum fluxes.

The term X_{P_M} (X_{P_E}) denotes the change rate of MAPE (EAPE) due to vertical mixing, heat, and freshwater fluxes. The term X_{K_M} (X_{K_E}) denotes the change rate of MKE (EKE) due to friction, wind stress, and bottom drag. These X terms are not explicitly diagnosed, as certain variables (e.g., temporally/spatially varying viscosity and diffusivity) are not available. The R terms and the vertical advection of APE are additional terms with higher-order Rossby numbers, which do not exist in the quasigeostrophic framework (Pedlosky 1987; von Storch et al. 2012). These terms can be neglected below the surface mixed layers and away from convective regions and are not further dealt with here.

c. Local versus nonlocal eddy–mean flow interaction

Figure 1 illustrates our definition of *local* eddy–mean flow interaction and *nonlocal* eddy–mean flow interaction. Summing Eqs. (7) and (9), and then integrating over an oceanic region, the rate of energy released from the mean flow through eddy–mean flow interaction is

$$\int_V(-D_{P_M}-M_{K_M})\,dv. \tag{12}$$

The pathways of the released energy [Eq. (12)] can be illustrated through the integral of the sum of Eqs. (7)–(10) over the region, that is,

$$\frac{\partial}{\partial t}\int_V(K_M+K_E+P_M+P_E)\,dv = \int_V(D_{P_M}+D_{P_E}+M_{K_M}+M_{K_E})\,dv+\text{Res}. \tag{13}$$

The variable Res represents all the other terms. The D and M terms on the right-hand side of Eq. (13) are the change rates of total kinetic and available potential energy due to eddy–mean flow interaction. They have divergence forms, that is,

$$\int_V(D_{P_M}+D_{P_E})\,dv=\int_V\nabla_H\cdot\left(\overline{\mathbf{u}'_H\rho'}\frac{g}{n_0}\overline{\rho^*}\right)dv, \tag{14}$$

and

$$\int_V(M_{K_M}+M_{K_E})\,dv=-\int_V\rho_0[\nabla\cdot(\overline{\overline{u}u'\mathbf{u}'})+\nabla\cdot(\overline{\overline{v}v'\mathbf{u}'})]\,dv. \tag{15}$$

If the magnitudes of the right-hand sides of Eqs. (14) and (15) are negligible, almost all the energy released from the mean flow is converted to eddy energy in the same region, and thus the eddy–mean flow interaction is *local* (Fig. 1b). If their magnitudes are not negligible, some energy released from the mean flow is not used to sustain the eddy growth in the same region, and the eddy–mean flow interaction is *nonlocal* (Fig. 1a). Note that Eqs. (14) and (15) have divergence forms, and thus their global integrals are zero.[1] Therefore, the part of the energy released from the mean flow that is not used to sustain the local eddy energy growth is essentially transported elsewhere through the divergence terms [Eqs. (14) and (15)], as illustrated in Fig. 1.

The energy route for eddy–mean flow interaction in the selected ocean regions is illustrated in Fig. 1a. Note that the horizontal arrows (D_{K_M} and D_{K_E} terms) occur with opposite signs in pairs in the energy budget equations, and therefore represent the exchange between the two energy reservoirs. However, the vertical arrows in red and blue do not appear with opposite signs in pairs, and energy divergence occurs, as indicated by the dashed lines in red and blue. Because their global integral vanishes, the dashed red and blue arrows shown in

[1] The global integral of $D_{P_M}+D_{P_E}$ is only approximately zero, as the vertical eddy density flux contribution is ignored (see the appendix).

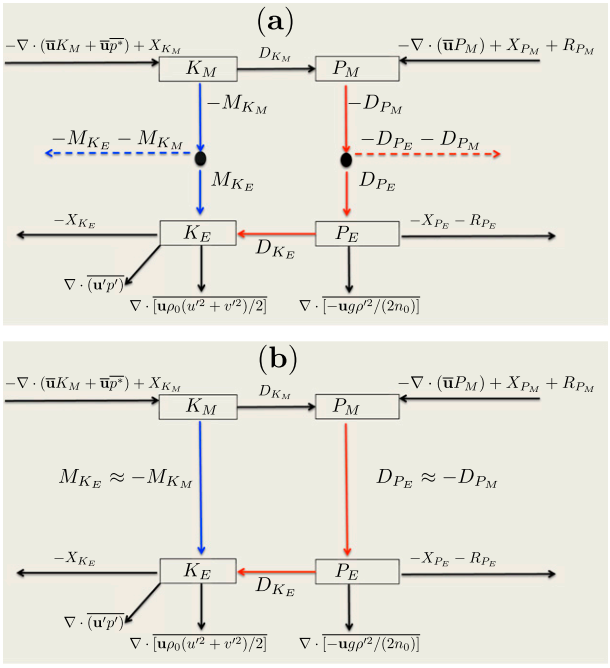

FIG. 1. Schematics illustrating the energy transfer through eddy–mean flow interaction (blue and red arrows). Other elements (black arrows) in the energy budgets are also included. Note that each term in these two diagrams essentially represents the volume integral of the term over the selected region from the ocean surface to the bottom. (a) The case when eddy–mean flow interaction is nonlocal. Only part of the energy released from the unstable mean flow through terms M_{K_M} and D_{P_M} is used to support the local eddy growth; the rest of the energy released is transported elsewhere through the divergence terms $M_{K_E}+M_{K_M}$ and $D_{P_E}+D_{P_M}$. (b) The case when eddy–mean flow interaction is local: the divergence terms are approximately zero, and thus all the energy released from the unstable mean flow through eddy–mean flow interaction transfers to eddies in the same region.

Fig. 1a are not included in the traditional Lorenz energy diagram, which is used to illustrate the energy pathway in the global atmosphere or ocean (e.g., Lorenz 1955; von Storch et al. 2012).

Nonlocal terms that do not concern eddy–mean flow interaction (i.e., advection and the work done by pressure work) also exist in the energy budgets. These nonlocal terms, in some cases, have noticeable magnitudes and contribute significantly to balancing the eddy–mean flow interaction terms. However, our definition of local and nonlocal eddy–mean flow interaction does not depend on the magnitude of these nonlocal terms.

3. The ECCO2 state estimate

a. Model configuration

To tackle the proposed questions using the diagnostic framework from the last section, we analyzed the 16-yr (1992–2007) solution averaged every 3 days from the Cube87 version of the ECCO2 state estimate. The ECCO2 state estimate is a free forward run using the Massachusetts Institute of Technology ocean general circulation model (Marshall et al. 1997a,b). The model solves hydrostatic and nonlinear primitive equations with the Boussinesq approximation in the global ocean on the cube-sphere grid (Adcroft et al. 2004). This eddy-permitting model has a mean horizontal resolution of 18 km and has 50 vertical levels with thicknesses varying from 10 to 456 m. It employs General Bathymetric Charts of the Ocean for the topography in the Arctic Ocean and uses the bathymetry data from Smith and Sandwell (1997) for the rest of the ocean (Menemenlis et al. 2008). Bottom stress is parameterized using the quadratic drag law. Biharmonic horizontal friction is used instead of Laplacian friction, and the *K*-profile parameterization (KPP) vertical mixing scheme from Large et al. (1994) is used to parameterize subgrid-scale vertical mixing processes.

Compared to other eddying models, the advantage of the ECCO2 state estimate is that it is a forward run using optimized control parameters (e.g., initial condition, surface forcing, background vertical viscosity, and bottom drag coefficient), which are calculated by reducing model–data misfits using the Green function approach (Menemenlis et al. 2005a,b, 2008). Thus, the solution is both realistic and dynamically consistent. Dynamical consistency makes the solution useful for process studies and budget diagnosis, as neither unphysical jumps nor artificial sources/sinks are introduced in the state estimate (Wunsch et al. 2009). Several previous studies of eddies using the ECCO2 state estimate (e.g., Volkov et al. 2008; Volkov and Fu 2008; Fu 2009) indicate the utility of the solution. More details are provided in Menemenlis et al. (2008) and Chen (2013).

b. Model fidelity about eddies and energetics

1) On the spatial pattern of eddy variability

The overall spatial features and magnitude of hydrographic variability and sea surface height variability in the ECCO2 state estimate are consistent with observations (Chen 2013). For example, the temperature variability at 250 m from both observations and the model is large in the Kuroshio Extension, the Gulf Stream Extension, the Antarctic Circumpolar Current, and the subtropical regions from the Pacific and Indian Oceans (Fig. 2). The model–data consistency for hydrographic variability is especially good in the upper ocean of mid- and low latitudes (not shown). Reasons are as follows: First, the dominant scale of eddies is closely related to the first baroclinic deformation radius, which is smaller

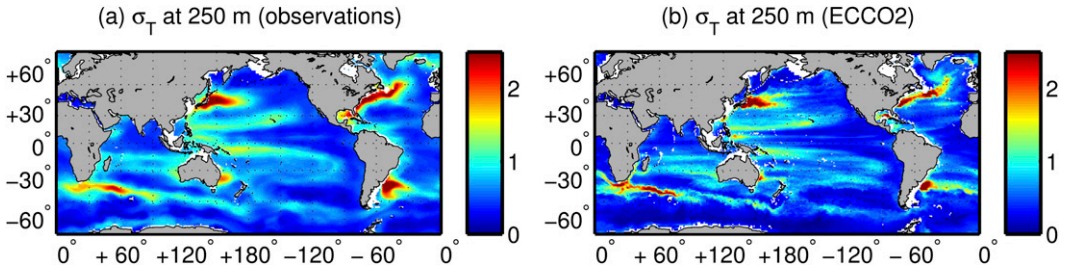

FIG. 2. Standard deviation of temperature (σ_T; °C) at 250 m (a) from observations in Forget and Wunsch (2007) and (b) from the ECCO2 state estimate. Seasonal variability is omitted in the standard deviation calculation.

in high latitudes; thus, the model grid is not fine enough to resolve motions on the deformation scale there. Second, the vertical resolution of the model is higher in the upper ocean than at depth, and the upper ocean is far from topographic features, some of which are too steep or too small scale for the model to represent accurately. Thus, the model performance in the deep ocean near topography may not be adequate. Third, fewer observations are available in the deep ocean and high latitudes, such as the Southern Ocean; thus, the model solution is less constrained there.

2) ON THE SPATIAL PATTERN OF ENERGETICS

Assessing the model fidelity concerning the eddy–mean flow interaction terms in Table 1 is challenging due to the lack of long-term density and velocity observations with three-dimensional coverage in large areas. One exception is the near-global long-term altimetric sea surface height data. The geostrophic contribution to M_{K_E} is

$$M_{K_E,\mathrm{geo}} = -\rho_0(\overline{u'_{\mathrm{geo}}\mathbf{u}'_{\mathrm{geo}}}\cdot\nabla_H\overline{u}_{\mathrm{geo}} + \overline{v'_{\mathrm{geo}}\mathbf{u}'_{\mathrm{geo}}}\cdot\nabla_H\overline{v}_{\mathrm{geo}}), \tag{16}$$

and a comparison with the model values is possible. The terms u_{geo} and v_{geo} are surface geostrophic velocities in the zonal and meridional directions, which can be obtained from sea surface height η, that is,

$$v_{\mathrm{geo}} = \frac{g}{f}\frac{\partial\eta}{\partial x} \quad \text{and} \quad u_{\mathrm{geo}} = -\frac{g}{f}\frac{\partial\eta}{\partial y}. \tag{17}$$

The spatial pattern of $M_{K_E,\mathrm{geo}}$ at the surface from the ECCO2 state estimate is similar to that from the altimetry in the off-equatorial regions (Fig. 3). Both maps show large magnitudes of $M_{K_E,\mathrm{geo}}$ in the western boundary currents and the Southern Ocean. Large magnitudes of $M_{K_E,\mathrm{geo}}$ in the Southern Ocean occur within roughly the same longitude ranges in these two maps. The zonally integrated values from the ECCO2 state estimate and altimetry are also very similar in the off-equatorial regions: both having peaks at 40°S, 25° and 35°N (not shown).

Both positive and negative values exist in the Southern Ocean and western boundary extension regions, though their detailed locations are only roughly the same in the two maps. We also computed $M_{K_E,\mathrm{geo}}$ using the 8-yr altimetry and ECCO2 state estimate (1993–2000). The location of these positive/negative spots based on the short record is the same as those based on the long record in roughly 80% of the global ocean. The correlation between the short-record and the long-record estimate is 0.9 in the ECCO2 state estimate, and it is 1 in the estimation based on altimetry.

3) ON THE GLOBALLY INTEGRATED VALUES

A growing body of literature focuses on the sources and sinks of kinetic energy, such as wind power input and dissipation through bottom drag, as reviewed in Ferrari and Wunsch (2009). Table 2 compares the globally integrated

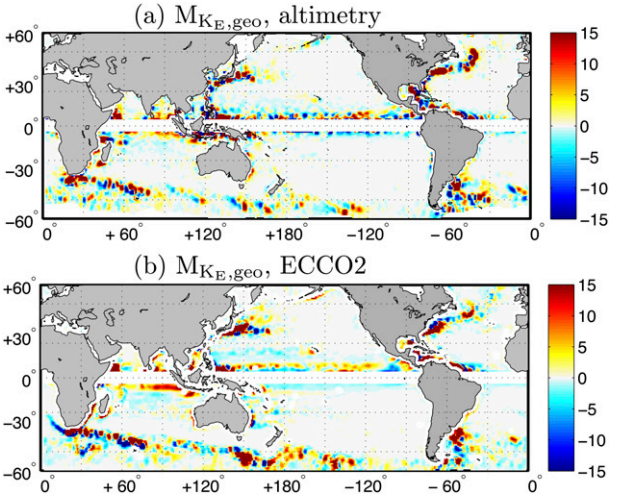

FIG. 3. The smoothed $M_{K_E,\mathrm{geo}}$ (10^{-6} W m^{-3}) using the (a) weekly sea surface height during 1993–2007 from the altimeter and (b) from the ECCO2 state estimate. Both patterns are dominated by large values in the western boundary currents and the Southern Ocean, and both are patchy in the Southern Ocean. The smoother is the 3° running average. The concept of $M_{K_E,\mathrm{geo}}$ breaks down at the equator due to the vanishing of the Coriolis parameter there. Thus, regions within 3° of the equator are masked.

TABLE 2. The 16-yr average of the globally integrated energy terms from the ECCO2 state estimate and previous studies. The term τ_s is wind stress, $\mathbf{u}_{\text{geo}}$ is the surface geostrophic velocity, $\boldsymbol{\tau}_b$ is the bottom drag based on the quadratic drag law, and $\mathbf{u}_b$ is bottom velocity. The global integral of the wind power input excludes the equatorial region (within ±3° of the equator), but the global integrals of other terms listed include the equatorial region. The errors shown are one standard error $\sigma/\sqrt{N}$, where σ is the standard deviation and N is the number of degrees of freedom. Assuming the time series is normally distributed, N is $M/\max[\sum_{n=-N_0}^{N_0} C(n)]$, where M is the number of points in the time series and $C(n)$ is the autocorrelation function of the time series. Two standard errors correspond to 95% confidence level.

Energy terms	Estimates from ECCO2 (TW)	Previous estimates (TW)
D_{K_E}	0.31 ± 0.01	0.2–0.8 from Wunsch and Ferrari (2004); 0.3 from Ferrari and Wunsch (2009).
$\tau_s \cdot \mathbf{u}_{\text{geo}}$	0.81 ± 0.02	0.88 from Wunsch (1998); 0.75–0.9 from Scott and Xu (2009).
$\boldsymbol{\tau}_s' \cdot \mathbf{u}_{\text{geo}}'$	0.12 ± 0.00	0.04–0.06 from Zhai et al. (2012); 0.04 from Wunsch (1998).
$\boldsymbol{\tau}_b \cdot \mathbf{u}_b$	0.03 ± 0.00	At least 0.2 from Sen et al. (2008); 0.14–0.65 from Arbic et al. (2009).

values from the ECCO2 state estimate with those in previous studies based on observations, models, and parameterization schemes. The global integrals of D_{K_E} and the wind power input into the surface geostrophic flow ($\tau_s \cdot \mathbf{u}_{\text{geo}}$) are consistent with previous estimates. Work done by the fluctuating winds ($\tau_s' \cdot \mathbf{u}_{\text{geo}}'$) may be overestimated in the ECCO2 state estimate.

Bottom drag dissipation ($\tau_b \cdot \mathbf{u}_b$) in the ECCO2 state estimate may be underestimated to some extent (Table 2). Consistently, Wortham (2013) found that the total kinetic energy in the ECCO2 state estimate below 2000 m at the mooring sites is approximately half of the kinetic energy observed from the current meters. On the other hand, differences in estimation methods probably also contribute to the difference between our estimates and previous ones for bottom drag dissipation. Sen et al. (2008) estimated the bottom drag dissipation using mooring observations, which are very sparse in space. Arbic et al. (2009) estimated the bottom drag dissipation from the snapshot bottom velocity in oceanic models, which includes the high-frequency component. The present estimate is calculated from the 3-day-averaged bottom velocity.

c. *On the length of the record*

Another question is whether the 16-yr record available from the ECCO2 state estimate is long enough to evaluate the eddy–mean flow interaction terms listed in Table 1. These terms involve eddy momentum and density fluxes. Our analysis suggests that the large-scale patterns and magnitude of time-mean eddy fluxes from the 16-yr record is remarkably similar to those estimated from shorter records. For example, D_{K_E} (the time-mean vertical eddy density flux multiplied by $-g$) estimated from the 1992–97 output and that from the 1992–2007 output in the global ocean have a spatial correlation of 0.8. Globally integrated D_{K_E} from the 6- and 16-yr records are both 0.3 TW. Figure 4 shows the comparison in the Kuroshio Extension region. The magnitude of the two patterns is almost the same. The large-scale features survive even in the estimates using the 6-yr record; D_{K_E} is positive (negative) in the western (eastern) part of the extension regions. Similarly, Greatbatch et al. (2010) found that the characteristics of surface momentum fluxes at the Kuroshio and Gulf Stream Extension regions estimated using a 5-yr altimetric dataset are similar to those estimated from the 13-yr record. Therefore, the 16-yr record is probably long enough to characterize the large-scale features of the global energetics patterns.

Small-scale variability also exists in the estimate based on the 16-yr record (e.g., Fig. 4). Oceanic motions and the associated hydrographic field have a wide range of spatial scales at all available frequencies (Wortham and

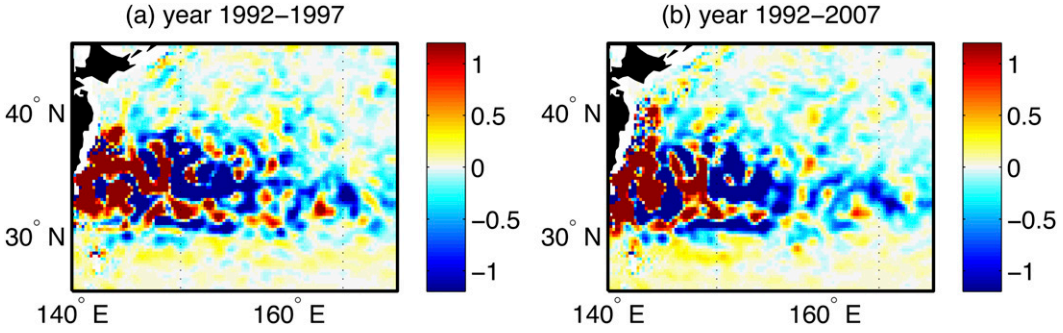

FIG. 4. The term D_{K_E} (10^{-5} W m^{-3}) at 550 m in the Kuroshio Extension region, estimated from the (a) 6- and (b) 16-yr ECCO2 state estimate.

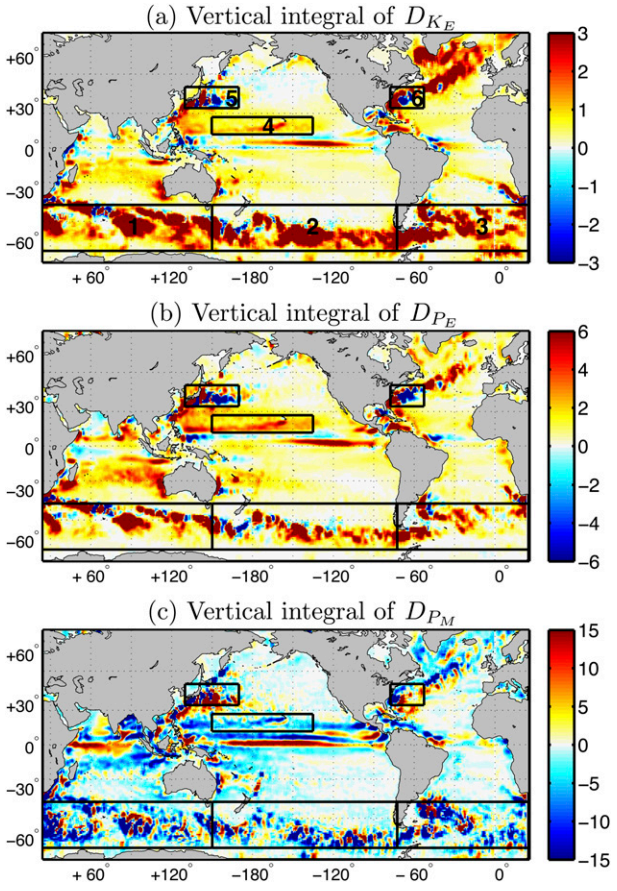

FIG. 5. The 3° running-averaged (a) D_{K_E}, (b) D_{P_E}, and (c) D_{P_M} integrated over the whole water column (10^{-3} W m^{-2}). These terms describe energy change rates due to eddy–mean flow interaction through eddy density fluxes (Table 1). Positive (negative) D_{P_E} (D_{P_M}) means eddies (mean flow) gain (releases) potential energy through this process. Positive D_{K_E} means EAPE is converted to EKE. Magnitudes in the six black boxes are large. Energy routes in regions indicated by the six boxes are discussed in section 4b.

Wunsch 2014), as a result of eddy–eddy interaction, instability, and the wide range of spatial scales in external forcing, topography, coastlines, etc. Therefore, small-scale features should exist in the time-mean eddy fluxes. The amplitude, position, and structures of these small-scale features will probably change as the record length increases. Detailed description and understanding of these small-scale features are left for future work.

4. Results

a. Global pattern of eddy–mean flow interaction

Figure 5 shows the spatial pattern of eddy–mean flow interaction due to eddy density fluxes [the D terms in Eqs. (8)–(10)]. The patterns of magnitudes are dominated by large values in the Southern Ocean, north of 40°N in the Atlantic basin, in the western boundary current regions, and in the subtropical gyre. In most of these areas, eddies grow through the interaction with the mean flow ($D_{P_E} > 0$) and the mean flow releases APE by interacting with eddies ($D_{P_M} < 0$). However, in the eastern part of the Kuroshio and Gulf Stream extension regions, eddies lose energy and the mean flow gains it.

The overall pattern of D_{K_E} in the North Atlantic is consistent with that in Zhai and Marshall (2013). Von Storch et al. (2012) presented the spatial pattern of D_{K_E} and D_{P_E} from a 0.1° global simulation. Though their time-varying flow includes variability with periods from 10 min to 10 yr and our time-varying flow includes variability with periods from 3 days to 16 yr, the spatial patterns of the vertically integrated D_{K_E} and D_{P_E} in this study are similar to theirs: values are large in the Southern Ocean and western boundary currents and are small in the subpolar gyres, and negative spots occur in the western bounder extension regions.

The similarity between the D_{K_E} and D_{P_E} patterns in Fig. 5 suggests that part of D_{P_E} transfers to EKE through the term D_{K_E}, which is consistent with baroclinic instability theory (Pedlosky 1987). However, the globally integrated D_{P_E} (0.5 TW) is larger than the globally integrated D_{K_E} (0.3 TW). Thus, only part of the energy extracted by EAPE from MAPE is used to support the EKE growth, and the remaining part is used to balance other terms in the EAPE budget. The complete pathway of EAPE in the ocean and realistic eddying models is still largely unknown.

Figure 6 shows the spatial pattern of vertically integrated eddy–mean flow energy exchanges due to eddy momentum fluxes [the M terms in Eqs. (7)–(8)]. The patterns show large magnitudes in the western boundary currents and the Southern Ocean and small values elsewhere. Eddies gain kinetic energy in most areas of the western boundary currents and many spots in the Southern Ocean ($M_{K_E} > 0$), but they lose kinetic energy in many places in the Southern Ocean ($M_{K_E} < 0$). The term M_{K_M} also has a sequence of positive and negative values in the Southern Ocean. This phenomenon has been identified in previous observation and modeling studies (e.g., Johnson et al. 1992; Morrow et al. 1992; Wilkin and Morrow 1994).

From a global integral perspective, eddies gain kinetic energy through M_{K_E} at 0.1 TW, and the mean flow releases kinetic energy through M_{K_M} at the same rate. To put this number into context, it is roughly 12% of the wind power input into the time-mean surface geostrophic flow, and it is one-third of the globally integrated D_{K_E}. In an oceanic region, part of the wind

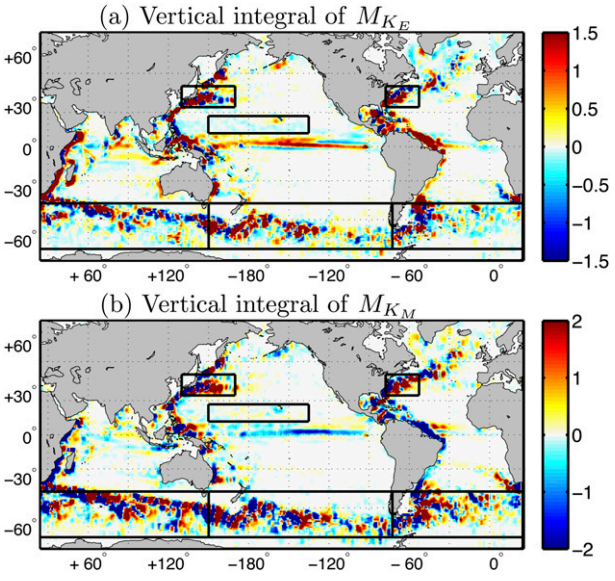

FIG. 6. The 3° running-averaged (a) M_{K_E} and (b) M_{K_M} integrated over the whole water column (10^{-3} W m^{-2}). These two terms are about the energy change rates due to eddy–mean flow interaction through eddy momentum fluxes (Table 1). Positive (negative) M_{K_E} (M_{K_M}) means eddies (mean flow) gain (releases) kinetic energy through this process. Their magnitudes are large in the western boundary currents and the Southern Ocean.

power input into geostrophic flow is converted to potential energy (Roquet et al. 2011) and then can be released from MAPE through D_{P_M} and sustain the eddy growth. The other part of the wind power input is transformed to pressure work (Roquet et al. 2011), which can change the local MKE budget and influence the energy released from MKE through M_{K_M}. Our calculation suggests that a major portion of the wind power input is used to sustain the D_{P_M} and D_{P_E} terms, but the contribution of the wind power input to the M terms is also not negligible.

b. *Regional energy routes of eddy–mean flow interaction*

Energy routes differ regionally from their global averages. The key diagram for the regional energy routes is Fig. 1a. Our results presented below are based on the 16-yr model output, though results from the 6-yr output (1992–97) are almost the same. Our results are also insensitive to the slight shift of the selected domain in either zonal or meridional direction on eddy scales (e.g., 1°).

1) SOUTHERN OCEAN

The Southern Ocean receives more than 75% of the total global wind power input (Roquet et al. 2011). The surface westerly wind stress in the Southern Ocean drives surface water northward, and thus the water below the surface is brought upward to conserve mass. Isopycnals are thus tilted upward toward the pole, and the Deacon cell meridional overturning circulation is formed and further maintained by the surface buoyancy forcing (e.g., Döös and Webb 1994; Marshall and Radko 2003; Thompson 2008). These previous studies agree that available potential energy stored in these tilted isopycnals can be released and used to generate eddies through baroclinic instability. On the other hand, previous observation and modeling work suggests that eddies generated through baroclinic instability in the Southern Ocean can intensify the mean flow through the convergence of eddy momentum fluxes ($M_{K_M} > 0$) in some regions and decelerate the mean flow through the opposite process ($M_{K_M} < 0$) in some other regions (e.g., McWilliams et al. 1978; Johnson et al. 1992; Morrow et al. 1992; Wilkin and Morrow 1994; Lenn et al. 2011).

Eddy–mean flow interaction in the Southern Ocean in the ECCO2 state estimate is consistent with studies summarized above in three aspects. First, in the ECCO2 state estimate, energy is released from the mean available potential energy stored in the tilted isopycnals, and eddies are generated ($D_{K_E} > 0$ and $D_{P_M} < 0$). Second, the gain rate of EKE from EAPE (D_{K_E}) in the Southern Ocean is roughly half of its globally integrated value. Third, eddies drive the mean flow through eddy momentum fluxes in some patches ($M_{K_M} > 0$) and decelerate the mean flow in some other patches ($M_{K_M} < 0$).

We also identify several new aspects about the eddy–mean flow interaction in the Southern Ocean (65°–40°S), summarized in Fig. 7. First, the negative and positive patches of M_{K_M} integrated over the three Southern Ocean boxes shown in Fig. 6 mostly cancel. The contribution of M_{K_E} to the eddy growth in the Southern Ocean is an order of magnitude smaller than the contribution of D_{P_E}. Second, energy released from the mean flow through D_{P_M} is about 250 GW, but only about 160 GW transfers to the EAPE reservoir through the term D_{P_E}. Thus, two-thirds of the energy released from the available potential energy stored in the tilted time-mean isopycnals are used to support the eddy growth in the Southern Ocean, and the rest of it is transported out of the domain through the divergence term $D_{P_M} + D_{P_E}$. This indicates that eddy–mean flow interaction in the Southern Ocean is nonlocal to some extent. The nonlocal nature arises from the spatial inhomogeneity of the eddy density fluxes and the mean flow, as

$$D_{P_M} + D_{P_E} = \frac{g}{n_0} \nabla_H \cdot (\overline{\mathbf{u}'_H \rho'} \, \overline{\rho^*}) \neq 0.$$

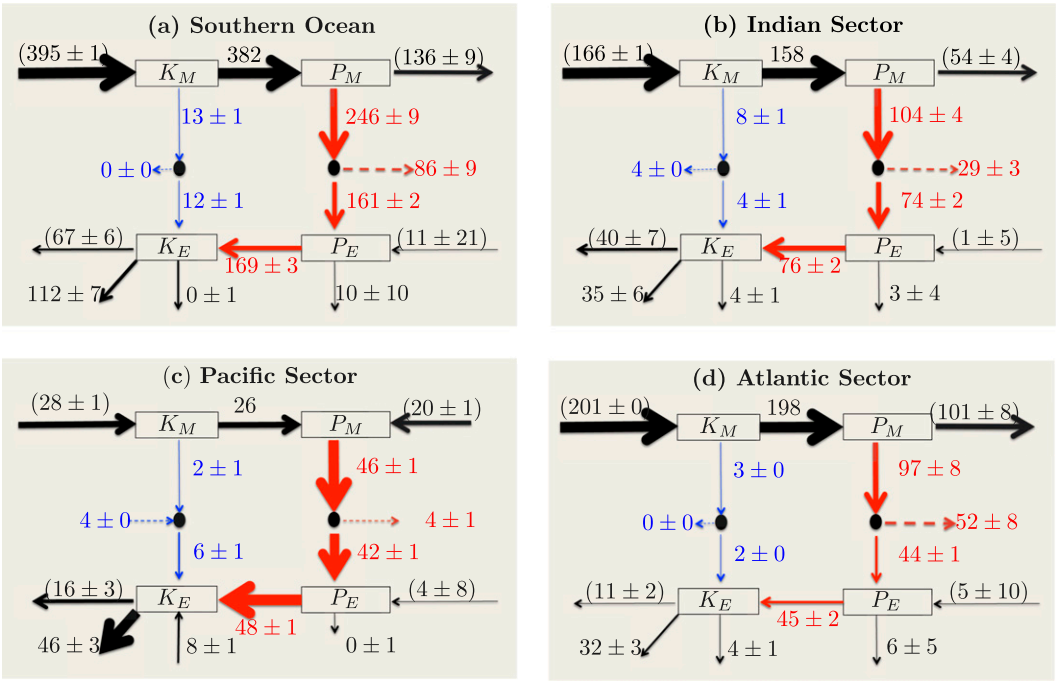

FIG. 7. The energy diagram in 10^9 W (GW) (Fig. 1) in the (a) whole Southern Ocean, (b) the Indian sector, (c) the Pacific sector, and (d) the Atlantic sector. These three sectors are, respectively, region 1, region 2, and region 3 in Fig. 5a. The whole Southern Ocean here denotes the sum of the three sectors. The contribution of the M terms to eddy growth is negligible. In the Indian and Atlantic sectors, only part of the energy released from MAPE through eddy–mean flow interaction supports the eddy energy growth in the same domain. In the Pacific sector, roughly all the MAPE released supports eddy energy growth in the same domain. Errors shown here are one standard error, as that in Table 2. We obtain the numbers in brackets from the residuals. These residuals also include the contribution of high-frequency motions to other terms in the energy budgets, since we use 3-day-averaged fields. Note that the time mean of the temporal change rate term is either zero or negligible and is not presented here. The imbalances, if they exist, are from the time mean of the temporal change rate term and the roundoff errors.

Both the mean flow, dominated by fronts and jet features, and the time-mean observed eddy heat fluxes in the Southern Ocean have rich small-scale variations (e.g., Lenn et al. 2011).

The energy routes in the Indian sector (65°–40°S, 25°–150°E), the Pacific sector (65°–40°S, 150°E–73°W), and the Atlantic sector (65°–40°S, 73°W–25°E) of the Southern Ocean are not entirely the same (Fig. 7). In all the three sectors, the contribution of the M terms to the eddy growth is negligible compared to the contribution of the D terms. In the Indian sector (Atlantic sector), roughly 70% (45%) of the energy released from the MAPE reservoir is used to sustain the eddy growth in the same region; in the Pacific sector, however, roughly 90% of the energy released from the MAPE reservoir is used to sustain the eddy growth in the same sector. The mechanism for the differences between these sectors is still to be determined. We also find that, compared to eddy–mean flow interaction through eddy density fluxes, advection contributes much less to the change of eddy energy. The EKE loss rate through pressure work and that through X_{K_E} are on the same order of magnitude.

2) SUBTROPICAL GYRES

Figure 8 shows the energy route through eddy–mean flow interaction in a midocean patch in the subtropical gyre (10°–22°N, 150°E–135°W). In this region, eddy–mean flow interaction due to eddy momentum fluxes is negligible (the M terms are effectively zero). Approximately all the energy released from MAPE is used to sustain the local EAPE growth, and little energy is exported elsewhere through $D_{P_M} + D_{P_E}$. Thus, eddy–mean flow interaction in this patch is local and consistent with the local assumption used in previous studies (e.g., Gill et al. 1974; Arbic and Flierl 2004; Tulloch et al. 2011). The EKE change rate due to advection in this region is 0 GW, and the dominant EKE sink is pressure work, not X_{K_E}. About 35% of D_{P_E} balances D_{K_E} and 15% of D_{P_E} balances the advection of EAPE. Whether results in this patch are representative of the subtropical gyres in other ocean basins is to be determined.

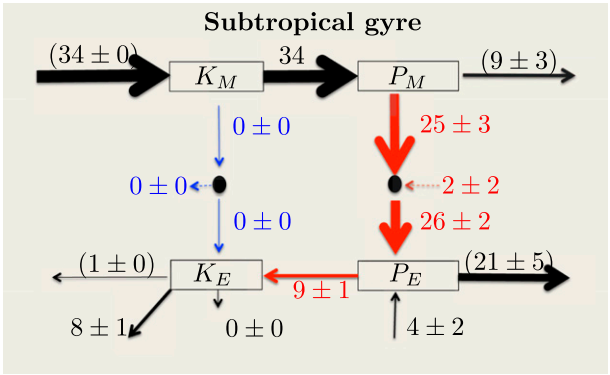

FIG. 8. As in Fig. 7, but for the subtropical gyre region (i.e., region 4 denoted in Fig. 5a). Eddy–mean flow interaction in this region is local.

3) WESTERN BOUNDARY EXTENSIONS

Figures 9a and 9b show the energy routes in the Kuroshio Extension (29°–42°N, 130°–170°E) and the Gulf Stream Extension regions (29°–42°N, 78°–53°W). The energy routes in these two regions are different from those in the Southern Ocean and the subtropical gyre in that the contribution of the M term to EKE growth is of the same order of magnitude as the contribution of the D term. Energy inputs through the boundaries in these two regions ($D_{P_M} + D_{P_E}$) are also not negligible. Consistency between our results with previous observation, modeling, and theoretical studies (e.g., Nishida and White 1982; Hall 1991; Eden et al. 2007; Waterman and Jayne 2011; Zhai and Marshall 2013) in the following aspect indicates that the regional energy routes here are reasonable: D_{K_E} is positive in the western part of the extension and negative in the eastern part, whereas M_{K_M} is positive in the eastern part of the extension and negative in the western part (Figs. 5, 6).

In the Kuroshio Extension region, energy is transferred from MAPE to EAPE with some energy input from the boundaries of the region and a small portion being converted to EKE (Fig. 9a). More detailed examination shows that the energy pathway in Fig. 9a is essentially the average of two different dynamical regimes shown in Figs. 9c and 9d. In the western half, energy is transferred from both the MKE and MAPE reservoirs to the eddy energy reservoir. The energy input from other regions is small, and the eddy–mean flow interaction is approximately local. By contrast, energy in the eastern half is converted from EAPE to MAPE; however, this is not the local baroclinic instability mechanism operating in reverse, as a large portion of the energy fed into MAPE is supplied from elsewhere through the divergence term and most of the EAPE loss to MAPE is not supplied by the local EKE reservoir. Note that, compared to the energy route in the eastern half, the energy route in the western half resembles more the energy route for the whole Kuroshio Extension region.

Using 2-yr mooring data at one site (35°N, 152°E) in the Kuroshio Extension region, Hall (1991) found that $D_{K_E} < 0$ and $D_{P_E} < 0$ at 350 dbar, and M_{K_E} is generally negative at this site. Waterman and Jayne (2011) found that by analyzing the potential vorticity and enstrophy budgets in an idealized two-layer model, eddies can drive the mean flow in the eastern part of the Kuroshio Extension through nonlinear eddy rectification processes due to localized forcing. In contrast to Waterman and Jayne (2011), we find that both eddies and the energy input through the boundaries contribute to the APE increase in the mean flow in the eastern part of the Kuroshio Extension region (Fig. 9). A complete theory of the energy pathways in Fig. 9 does not exist. Whether these energetic features exist in the instability processes due to localized forcing (e.g., pulse instabilities) is still not known (e.g., Farrell 1982; Helfrich and Pedlosky 1993, 1995).

5. Conclusions and discussion

Our main findings are that 1) energetics of eddy–mean flow interaction processes vary strongly geographically, and 2) both local and nonlocal eddy–mean flow interactions exist in the ocean. The mean flow releases energy through eddy–mean flow interaction in most regions, but gains energy in other regions. Interactions due to eddy density fluxes are pronounced in the Southern Ocean, western boundary extension regions, and the subtropical gyres, while interactions due to eddy momentum fluxes play a large role in the Southern Ocean and western boundary current regions. The interaction is approximately local in the selected subtropical gyre region, but it is nonlocal in the Southern Ocean, where the oceanic circulation is less spatially homogeneous. Energetics in the eastern half and the western half of the Kuroshio Extension region are very different. In the western half, the mean flow is both baroclinically and barotropically unstable, and most energy released from the mean flow transfers to eddies; in the eastern half, eddy energy transfers back to the mean flow, and eddy–mean flow interaction is nonlocal, as the divergence terms are nonnegligible. Pressure work acts as a nonnegligible sink of EKE in all the selected regions.

The results summarized above are not definitive and come with several caveats. First, the ECCO2 state estimate does not resolve submesoscale variability, and the fidelity of the mesoscale variability from the state

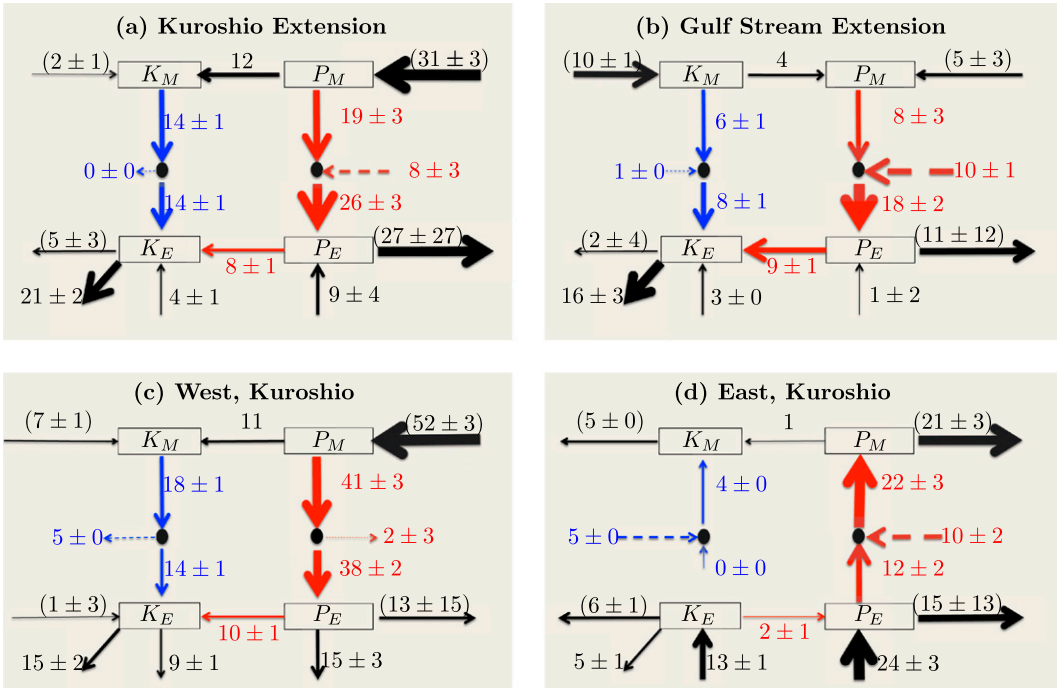

FIG. 9. As in Fig. 7, but for the (a) Kuroshio Extension region, (b) Gulf Stream Extension region, and (c) western half and (d) eastern half of the Kuroshio Extension region. The Kuroshio Extension and Gulf Stream Extension regions are, respectively, region 5 and region 6 in Fig. 5a. In (a) and (b), the contribution of D and M terms to the eddy growth is on the same order of magnitude. In (c), energy is transferred from the mean flow to eddies through both the D and M terms; in (d), energy is transferred from EAPE to MAPE.

estimate remains partially uncertain. Other numerical models may provide different descriptions. Second, an important assumption here is that the 16-yr model output is long enough to separate the putative time-mean flow from the oceanic variability. Finally, the definition of APE is arguable, but we assume that the definition based on the quasigeostrophic form is reasonable enough for this study. Note that this definition may not represent the true total amount of APE (which is not the concern here); that could be obtained through adiabatic adjustment (Huang 2005). But a new diagnostic framework for the EAPE and MAPE budgets would need to be developed. We speculate that D_{P_M} and D_{P_E} depend weakly on the APE definition; however, D_{K_E} does not, as it is directly derived from the EKE budget.

These findings also raise some puzzles. In the current estimate, one-third of the energy released from the APE in the mean flow in the Southern Ocean moves to other regions through the divergence term. Assuming this result is not sensitive to the model resolution, record length, and diagnostic framework, it is important to study the causes of the nonlocal nature of eddy–mean flow interaction and the consequences of this nonlocal nature in various aspects, such as jet behaviors, eddy characteristics, and spatial structures of eddy mixing rates.

Besides this work, a related yet distinct study (i.e., Grooms et al. 2013) has also been carried out recently to discuss "eddy energy locality." Both studies point out the prevalence of eddy energy nonlocality and indicate the need of using nonlocal eddy parameterization schemes. However, these two studies have a few differences. First, this study introduced the concept of eddy energy nonlocality caused by eddy–mean flow interaction. The nonlocality due to advection and pressure work [divergence terms on the left-hand sides of Eqs. (7)–(10)] are not our focus. Their study focused on the eddy energy nonlocality due to the combination of all available nonlocal processes in their model (i.e., the total divergence of energy flux in the energy budget). Second, they define eddies as motions with small spatial scales and focus on quasigeostrophic flows in an idealized wind-driven basin. We define eddies as deviation from a time mean and employ a global eddy-permitting ocean state estimate for our analysis.

All types of eddy definition exist, such as coherent vortices, deviation from a time mean or zonal mean, and mesoscale motions (Grooms et al. 2013). Our eddy definition, deviation from a time mean, is widely used in

the previous literature (e.g., Wunsch 1998; von Storch et al. 2012; Zhai and Marshall 2013). Though it is not directly related to subgrid-scale parameterization, it allows us to develop the simplest possible framework to illustrate the concept of local versus nonlocal eddy–mean flow interaction. Future work is needed to extend this study to other eddy definitions.

Some other possible future tasks are 1) to develop a diagnostic framework based on a more accurate definition of available potential energy, 2) to diagnose the vorticity, enstrophy, and momentum budgets to have a more complete description of eddy–mean flow interaction in the global ocean, and 3) to partition the contribution of oceanic variability at different spatial and time scales to eddy–mean flow interaction.

Acknowledgments. Most material was from a Ph.D. thesis from the MIT–WHOI Joint Program in Oceanography (i.e., Chen 2013). R. Chen thanks NASA (NNX09AI87G and NNX08AR33G) for support. Remarks from Shafer Smith and one anonymous reviewer greatly improved the paper. We thank J.-M. Campin, C. Hill, D. Menemenlis, and H. Zhang for discussions about the ECCO2 state estimate. R. Chen's thesis committee (R. Ferrari, R. Huang, S. Lentz, J. Marshall, and M. Spall) provided helpful suggestions. Comments from A. Wang improved the presentation of the energy diagram.

APPENDIX

Derivation of the Energy Equations

a. Governing equations for kinetic energy

The momentum equations in the x and y directions in the ECCO2 state estimate are

$$\frac{\partial u}{\partial t}+\nabla\cdot(u\mathbf{u})-fv=-\frac{1}{\rho_0}\frac{\partial}{\partial x}p+D_u,\quad\text{and}\tag{A1}$$

$$\frac{\partial v}{\partial t}+\nabla\cdot(v\mathbf{u})+fu=-\frac{1}{\rho_0}\frac{\partial}{\partial y}p+D_v,\tag{A2}$$

where

$$D_u=\frac{\partial}{\partial z}A_z\frac{\partial u}{\partial z}+A_4\nabla_h^4u\quad\text{and}\quad D_v=\frac{\partial}{\partial z}A_z\frac{\partial v}{\partial z}+A_4\nabla_h^4v,\tag{A3}$$

respectively, denoting the momentum change rates in the x and y directions due to friction. The term p is the hydrostatic pressure, $\nabla\cdot$ is the divergence operator, A_z is vertical viscosity, A_4 is horizontal biharmonic viscosity, and $\mathbf{u}$ is the three-dimensional velocity vector.

Following von Storch et al. (2012), multiply Eqs. (A1) and (A2) by u' and v', respectively, sum them together, and perform a temporal average to obtain the equation for EKE:

$$\begin{aligned}\frac{\partial}{\partial t}K_E+\nabla\cdot\overline{\left[\mathbf{u}\frac{1}{2}\rho_0(u'^2+v'^2)\right]}+\nabla\cdot\overline{(\mathbf{u}'p')}\\=\underbrace{-g\overline{\rho'w'}}_{D_{K_E}}\ \underbrace{-\rho_0(\overline{u'\mathbf{u}'}\cdot\nabla\overline{u}+\overline{v'\mathbf{u}'}\cdot\nabla\overline{v})}_{M_{K_E}}\\+\underbrace{\rho_0(\overline{u'D_u'}+\overline{v'D_v'})}_{X_{K_E}}.\end{aligned}\tag{A4}$$

Multiply Eqs. (A1) and (A2) by $\overline{u}$ and $\overline{v}$, respectively, sum them together, and perform a temporal average to obtain the equation for MKE:

$$\begin{aligned}\frac{\partial}{\partial t}K_M+\nabla\cdot(\overline{\mathbf{u}}K_M)+\nabla\cdot(\overline{\mathbf{u}}\,\overline{p})=-g\overline{\rho}\,\overline{w}-\rho_0[\overline{u}\nabla\cdot(\overline{\mathbf{u}'u'})\\+\overline{v}\nabla\cdot(\overline{\mathbf{u}'v'})]+\rho_0(\overline{u}\overline{D_u}+\overline{v}\overline{D_v}).\end{aligned}\tag{A5}$$

Noting that under the hydrostatic approximation in the ECCO2 state estimate,

$$\nabla\cdot(\overline{\mathbf{u}}\,\overline{p})+g\overline{\rho}\,\overline{w}=\nabla\cdot(\overline{\mathbf{u}}\overline{p^*})+g\overline{\rho^*w},\tag{A6}$$

where $\cdot^*$ denotes the deviation of the variable [e.g., $p(x,y,z,t)$ and $\rho(x,y,z,t)$] from its time and global mean [e.g. $\langle p(x,y,z,t)\rangle$ and $\langle\rho(x,y,z,t)\rangle$]. Therefore, Eq. (A5) can be converted to

$$\begin{aligned}\frac{\partial}{\partial t}K_M+\nabla\cdot(\overline{\mathbf{u}}K_M)+\nabla\cdot(\overline{\mathbf{u}}\overline{p^*})\\=\underbrace{-g\overline{\rho^*w}}_{D_{K_M}}\ \underbrace{-\rho_0[\overline{u}\nabla\cdot(\overline{u'\mathbf{u}'})+\overline{v}\nabla\cdot(\overline{v'\mathbf{u}'})]}_{M_{K_M}}\\+\underbrace{\rho_0(\overline{u}\overline{D_u}+\overline{v}\overline{D_v})}_{X_{K_M}}.\end{aligned}\tag{A7}$$

b. Governing equations for available potential energy

To obtain the APE equations, first we derive the in situ density equation. The potential temperature θ and salinity S equations in the ECCO2 state estimate are

$$\frac{d\theta}{dt}=H_\theta,\quad\frac{dS}{dt}=H_S,\tag{A8}$$

where

$$\frac{d}{dt}=\frac{\partial}{\partial t}+\left(u\frac{\partial}{\partial x}+v\frac{\partial}{\partial y}+w\frac{\partial}{\partial z}\right).$$

The variable H_θ (H_S) denotes the change rate of temperature (salinity) due to the vertical mixing parameterized using the KPP scheme and air–sea exchange of heat (freshwater). Using Eq. (A8) and the equation of state in the ECCO2 state estimate [i.e. $\rho(x, y, z, t) = \rho(\theta, S, \rho_0 gz)$], we obtain

$$\frac{d\rho}{dt} = \left(\frac{\partial\rho}{\partial\theta}\right)_{S,z}\frac{d\theta}{dt} + \left(\frac{\partial\rho}{\partial\theta}\right)_{\theta,z}\frac{dS}{dt} + \left(\frac{\partial\rho}{\partial z}\right)_{S,\theta}\frac{dz}{dt} = H_\rho + w\widehat{\rho_z}, \tag{A9}$$

where

$$\widehat{\rho_z} = \left(\frac{\partial\rho}{\partial z}\right)_{S,\theta} \quad \text{and} \quad H_\rho = \left(\frac{\partial\rho}{\partial\theta}\right)_{S,z} H_\theta + \left(\frac{\partial\rho}{\partial S}\right)_{\theta,z} H_S. \tag{A10}$$

We decompose both ρ and $\widehat{\rho_z}$ into three parts, that is,

$$\begin{aligned}\rho(x, y, z, t) &= \langle\overline{\rho}\rangle(z) + \rho^*(x, y, z)\\ &= \langle\overline{\rho}\rangle(z) + \overline{\rho^*}(x, y, z) + \rho'(x, y, z, t), \quad \text{and}\end{aligned} \tag{A11}$$

$$\widehat{\rho_z}(x, y, z, t) = \langle\overline{\widehat{\rho_z}}\rangle(z) + \widehat{\rho_z}^*(x, y, z, t) = \langle\overline{\widehat{\rho_z}}\rangle(z) + \overline{\widehat{\rho_z}^*}(x, y, z) + \widehat{\rho_z}'(x, y, z, t). \tag{A12}$$

Substituting Eqs. (A11) and (A12) into Eq. (A9), we obtain the density equation for ρ^*:

$$\begin{aligned}&\frac{\partial}{\partial t}\rho^* + \nabla\cdot(\mathbf{u}\rho^*) + wn_0\\ &= \frac{\partial}{\partial t}(\overline{\rho^*} + \rho') + \nabla\cdot[\mathbf{u}(\overline{\rho^*} + \rho')] + wn_0 = H_\rho + w\widehat{\rho_z}^*,\end{aligned} \tag{A13}$$

where n_0 is defined in Eq. (4).

Multiply Eq. (A13) by $-g\overline{\rho^*}/n_0$ and then time average, we can get the MAPE equation:

$$\begin{aligned}\frac{\partial}{\partial t}P_M + \nabla\cdot(\overline{\mathbf{u}}P_M) = &\underbrace{\overline{\rho^*}\nabla\cdot\left(\overline{\mathbf{u}'\rho'\frac{g}{n_0}}\right)}_{D_{P_M,0}} + g\overline{\rho^*}\,\overline{w}\\ &- \frac{g}{n_0}\overline{\rho^*}\,\overline{H_\rho} + R_{P_{M0}},\end{aligned} \tag{A14}$$

where

$$R_{P_{M0}} = -P_M\cdot\frac{\overline{w}}{n_0}\frac{\partial n_0}{\partial z} - g\overline{\rho^*}\,\overline{w'\rho'}\frac{\partial}{\partial z}\left(\frac{1}{n_0}\right) - \frac{g}{n_0}\overline{\rho^*}\,\overline{w\widehat{\rho_z}^*}. \tag{A15}$$

Multiply Eq. (A13) by $-g\rho'/n_0$ and then time average, we can get the EAPE equation:

$$\begin{aligned}&\frac{\partial}{\partial t}P_E + \nabla\cdot\overline{[-\mathbf{u}g\rho'^2/(2n_0)]}\\ &= \underbrace{\overline{\mathbf{u}'\rho'\frac{g}{n_0}}\cdot\nabla\overline{\rho^*}}_{D_{P_E,0}} + g\overline{\rho'w'} - \frac{g}{n_0}\overline{\rho' H'_\rho} + R_{P_{E0}},\end{aligned} \tag{A16}$$

where

$$R_{P_{E0}} = \overline{g\rho'^2/(2n_0)\cdot\frac{w}{n_0}\frac{\partial n_0}{\partial z}} - \frac{g}{n_0}\overline{\rho' w\widehat{\rho_z}^*}. \tag{A17}$$

The terms $D_{P_E,0}$ and $D_{P_M,0}$ can be divided into a horizontal eddy density flux part and a vertical density flux part:

$$D_{P_E,0} = \underbrace{\overline{\mathbf{u}'_H\rho'\frac{g}{n_0}}\cdot\nabla_H\overline{\rho^*}}_{D_{P_E}} + \overline{w'\rho'\frac{g}{n_0}}\frac{\partial}{\partial z}\overline{\rho^*}, \quad \text{and} \tag{A18}$$

$$D_{P_M,0} = \underbrace{\overline{\rho^*}\nabla_H\cdot\left(\overline{\mathbf{u}'_H\rho'\frac{g}{n_0}}\right)}_{D_{P_M}} + \overline{\rho^*}\frac{\partial}{\partial z}\left(\overline{w'\rho'\frac{g}{n_0}}\right), \tag{A19}$$

where $\mathbf{u}_H$ is horizontal velocity, and ∇_H is the horizontal gradient operator. This study diagnoses D_{P_E} and D_{P_M} instead of $D_{P_E,0}$ and $D_{P_M,0}$; because D_{P_E} and D_{P_M} are involved in quasigeostrophic eddy dynamics and can be used to indicate baroclinic instability. Therefore, we write Eqs. (A14) and (A16) in the following form:

$$\begin{aligned}\frac{\partial}{\partial t}P_M + \nabla\cdot(\overline{\mathbf{u}}P_M) = &\underbrace{\overline{\rho^*}\nabla_H\cdot\left(\overline{\mathbf{u}'_H\rho'\frac{g}{n_0}}\right)}_{D_{P_M}}\\ &+ \underbrace{g\overline{\rho^*}\,\overline{w}}_{D_{K_M}} \underbrace{- \frac{g}{n_0}\overline{\rho^*}\,\overline{H_\rho}}_{X_{P_M}} + R_{P_M}, \quad \text{and}\end{aligned} \tag{A20}$$

$$\begin{aligned}&\frac{\partial}{\partial t}P_E + \nabla\cdot\overline{[-\mathbf{u}g\rho'^2/(2n_0)]}\\ &= \underbrace{\overline{\mathbf{u}'_H\rho'\frac{g}{n_0}}\cdot\nabla_H\overline{\rho^*}}_{D_{P_E}} \underbrace{- (-g\overline{\rho'w'})}_{D_{K_E}} \underbrace{- \frac{g}{n_0}\overline{\rho' H'_\rho}}_{X_{P_E}} + R_{P_E},\end{aligned} \tag{A21}$$

where

$$\begin{aligned}R_{P_M} &= R_{P_{M0}} + \overline{\rho^*}\frac{\partial}{\partial z}\left(\overline{w'\rho'\frac{g}{n_0}}\right),\\ R_{P_E} &= R_{P_{E0}} + \overline{w'\rho'\frac{g}{n_0}}\frac{\partial}{\partial z}\overline{\rho^*}.\end{aligned} \tag{A22}$$

The variable D_{K_M} denotes the exchange rate between MKE and MAPE.

The global integral of $D_{P_E} + D_{P_M}$ is

$$\int_V (D_{P_E} + D_{P_M})\, dV = \int_V \nabla_H \cdot \left(\overline{\mathbf{u}'_H \rho' \frac{g}{n_0}} \overline{\rho^*} \right) dV$$
$$= -\int_V \frac{\partial}{\partial z} \left(\overline{w' \rho' \frac{g}{n_0}} \overline{\rho^*} \right) dV, \qquad \text{(A23)}$$

where $\int_V \cdot\, dV$ denotes the global integral. It is a negligible number under quasigeostrophic assumption. In the ECCO2 state estimate, $\int_V (D_{P_E} + D_{P_M})\, dV$ is -0.07 TW, which is much smaller than $\int_V D_{P_E}\, dV$ (0.51 TW) and $\int_V D_{P_M}\, dV$ (-0.58 TW).

REFERENCES

Adcroft, A., J.-M. Campin, C. Hill, and J. Marshall, 2004: Implementation of an atmosphere–ocean general circulation model on the expanded spherical cube. *Mon. Wea. Rev.,* **132,** 2845–2863, doi:10.1175/MWR2823.1.

Arbic, B. K., 2000: Generation of mid-ocean eddies: The local baroclinic instability hypothesis. Ph.D. thesis, Massachusetts Institute of Technology and Woods Hole Oceanographic Institution, 290 pp.

——, and G. R. Flierl, 2004: Baroclinically unstable geostrophic turbulence in the limits of strong and weak bottom Ekman friction: Application to midocean eddies. *J. Phys. Oceanogr.,* **34,** 2257–2273, doi:10.1175/1520-0485(2004)034<2257:BUGTIT>2.0.CO;2.

——, and Coauthors, 2009: Estimates of bottom flows and bottom boundary layer dissipation of the oceanic general circulation from global high-resolution models. *J. Geophys. Res.,* **114,** C02024, doi:10.1029/2008JC005072.

Brown, J. N., and A. V. Fedorov, 2010: How much energy is transferred from the winds to the thermocline on ENSO time scales? *J. Climate,* **23,** 1563–1580, doi:10.1175/2009JCLI2914.1.

Chen, R., 2013: Energy pathways and structures of oceanic eddies from the ECCO2 state estimate and simplified models. Ph.D. thesis, Massachusetts Institute of Technology and Woods Hole Oceanographic Institution, 206 pp.

Cox, M., 1987: An eddy-resolving numerical model of the ventilated thermocline: Time dependence. *J. Phys. Oceanogr.,* **17,** 1044–1056, doi:10.1175/1520-0485(1987)017<1044:AERNMO>2.0.CO;2.

Döös, K., and D. Webb, 1994: The Deacon cell and the other meridional cells of the Southern Ocean. *J. Phys. Oceanogr.,* **24,** 429–442, doi:10.1175/1520-0485(1994)024<0429:TDCATO>2.0.CO;2.

Eden, C., R. J. Greatbatch, and J. Willebrand, 2007: A diagnosis of thickness fluxes in an eddy-resolving model. *J. Phys. Oceanogr.,* **37,** 727–742, doi:10.1175/JPO2987.1.

Farrell, B. F., 1982: Pulse asymptotics of the Charney baroclinic instability problem. *J. Atmos. Sci.,* **39,** 507–517, doi:10.1175/1520-0469(1982)039<0507:PAOTCB>2.0.CO;2.

Ferrari, R., and C. Wunsch, 2009: Ocean circulation kinetic energy: Reservoirs, sources and sinks. *Annu. Rev. Fluid Mech.,* **41,** 253–282, doi:10.1146/annurev.fluid.40.111406.102139.

——, and ——, 2010: The distribution of eddy kinetic and potential energies in the global ocean. *Tellus,* **62A,** 92–108, doi:10.1111/j.1600-0870.2009.00432.x.

Forget, G., and C. Wunsch, 2007: Estimated global hydrographic variability. *J. Phys. Oceanogr.,* **37,** 1997–2008, doi:10.1175/JPO3072.1.

Fu, L.-L., 2009: Pattern and velocity of propagation of the global ocean eddy variability. *J. Geophys. Res.,* **114,** C11017, doi:10.1029/2009JC005349.

——, and G. R. Flierl, 1980: Nonlinear energy and enstrophy transfers in a realistically stratified ocean. *Dyn. Atmos. Oceans,* **4,** 219–246, doi:10.1016/0377-0265(80)90029-9.

Gill, A. E., J. S. A. Green, and A. J. Simmons, 1974: Energy partition in the large-scale ocean circulation and the production of mid-ocean eddies. *Deep-Sea Res. Oceanogr. Abstr.,* **21,** 499–528, doi:10.1016/0011-7471(74)90010-2.

Greatbatch, R. J., X. Zhai, J. D. Kohlmann, and L. Czeschel, 2010: Ocean eddy momentum fluxes at the latitudes of the Gulf Stream and the Kuroshio Extensions as revealed by satellite data. *Ocean Dyn.,* **60,** 617–628, doi:10.1007/s10236-010-0282-6.

Grooms, I., L.-P. Nadeau, and K. S. Smith, 2013: Mesoscale eddy energy locality in an idealized ocean model. *J. Phys. Oceanogr.,* **43,** 1911–1923, doi:10.1175/JPO-D-13-036.1.

Hall, M. M., 1991: Energetics of the Kuroshio Extension at 35°N, 152°E. *J. Phys. Oceanogr.,* **21,** 958–975, doi:10.1175/1520-0485(1991)021<0958:EOTKEA>2.0.CO;2.

Held, I. M., and V. D. Larichev, 1996: A scaling theory for horizontally homogeneous, baroclinically unstable flow on a beta-plane. *J. Atmos. Sci.,* **53,** 946–952, doi:10.1175/1520-0469(1996)053<0946:ASTFHH>2.0.CO;2.

Helfrich, K. R., and J. Pedlosky, 1993: Time-dependent isolated anomalies in zonal flows. *J. Fluid Mech.,* **251,** 377–409, doi:10.1017/S0022112093003453.

——, and ——, 1995: Large-amplitude coherent anomalies in baroclinic zonal flows. *J. Atmos. Sci.,* **52,** 1615–1629, doi:10.1175/1520-0469(1995)052<1615:LACAIB>2.0.CO;2.

Huang, R. X., 2004: Ocean, energy flows in. *Encyclopedia of Energy,* C. J. Cleveland, Ed., Elsevier, 497–509, doi:10.1016/B0-12-176480-X/00053-X.

——, 2005: Available potential energy in the world's oceans. *J. Mar. Res.,* **63,** 141–158, doi:10.1357/0022240053693770.

——, 2010: *Ocean Circulation: Wind-Driven and Thermohaline Processes.* Cambridge University Press, 806 pp.

Johnson, T. J., R. H. Stewart, C. K. Shum, and B. D. Tapley, 1992: Distribution of Reynolds stress carried by mesoscale variability in the Antarctic Circumpolar Current. *Geophys. Res. Lett.,* **19,** 1201–1204, doi:10.1029/92GL01287.

Kundu, P. K., and I. M. Cohen, 2004: *Fluid Mechanics.* Elsevier Academic Press, 759 pp.

Kuo, A., R. A. Plumb, and J. Marshall, 2005: Transformed Eulerian-mean theory. Part II: Potential vorticity homogenization, and the equilibrium of a wind- and buoyancy-driven zonal flow. *J. Phys. Oceanogr.,* **35,** 175–187, doi:10.1175/JPO-2670.1.

Large, W., J. McWilliams, and S. Doney, 1994: Oceanic vertical mixing: A review and a model with a nonlocal boundary layer parameterization. *Rev. Geophys.,* **32,** 363–403, doi:10.1029/94RG01872.

Lenn, Y. D., T. K. Chereskin, J. Sprintall, and J. L. McClean, 2011: Near-surface eddy heat and momentum fluxes in the Antarctic Circumpolar Current in Drake Passage. *J. Phys. Oceanogr.,* **41,** 1385–1407, doi:10.1175/JPO-D-10-05017.1.

Liang, X. S., and A. R. Robinson, 2007: Localized multi-scale energy and vorticity analysis: II. Finite-amplitude instability theory and validation. *Dyn. Atmos. Oceans,* **44,** 51–76, doi:10.1016/j.dynatmoce.2007.04.001.

Lorenz, E. N., 1955: Available potential energy and the maintenance of the general circulation. *Tellus,* **7,** 157–167, doi:10.1111/j.2153-3490.1955.tb01148.x.

Margules, M., 1905: On the energy of storms. *Smithson. Misc. Collect.,* **51,** 533–595.

Marshall, J. C., 1984: Eddy-mean-flow interaction in a barotropic ocean model. *Quart. J. Roy. Meteor. Soc.,* **110,** 573–590, doi:10.1002/qj.49711046502.

——, and T. Radko, 2003: Residual-mean solutions for the Antarctic Circumpolar Current and its associated overturning circulation. *J. Phys. Oceanogr.,* **33,** 2341–2354, doi:10.1175/1520-0485(2003)033<2341:RSFTAC>2.0.CO;2.

——, A. Adcroft, C. Hill, L. Perelman, and C. Heisey, 1997a: A finite-volume, incompressible Navier Stokes model for studies of the ocean on parallel computers. *J. Geophys. Res.,* **102,** 5753–5766, doi:10.1029/96JC02775.

——, C. Hill, L. Perelman, and A. Adcroft, 1997b: Hydrostatic, quasi-hydrostatic, and nonhydrostatic ocean modeling. *J. Geophys. Res.,* **102,** 5733–5752, doi:10.1029/96JC02776.

McWilliams, J. C., W. R. Holland, and J. H. S. Chow, 1978: A description of numerical Antarctic Circumpolar Currents. *Dyn. Atmos. Oceans,* **2,** 213–291, doi:10.1016/0377-0265(78)90018-0.

Menemenlis, D., and Coauthors, 2005a: NASA supercomputer improves prospects for ocean climate research. *Eos, Trans. Amer. Geophys. Union,* **86,** 89–96, doi:10.1029/2005EO090002.

——, I. Fukumori, and T. Lee, 2005b: Using Green's functions to calibrate an ocean general circulation model. *Mon. Wea. Rev.,* **133,** 1224–1240, doi:10.1175/MWR2912.1.

——, J. Campin, P. Heimbach, C. Hill, T. Lee, A. Nguyen, M. Schodlock, and H. Zhang, 2008: ECCO2: High resolution global ocean and sea ice data synthesis. *Mercator Ocean Quarterly Newsletter,* No. 31, Mercator Ocean, Ramonville Saint-Agne, France, 13–21. [Available online at http://www.mercator-ocean.fr/eng/actualites-agenda/newsletter/newsletter-Newsletter-31-The-GODAE-project.]

Morrow, R., J. Church, R. Coleman, D. Chelton, and N. White, 1992: Eddy momentum flux and its contribution to the Southern Ocean momentum balance. *Nature,* **357,** 482–484, doi:10.1038/357482a0.

Nishida, H., and W. White, 1982: Horizontal eddy fluxes of momentum and kinetic energy in the near-surface of the Kuroshio Extension. *J. Phys. Oceanogr.,* **12,** 160–170, doi:10.1175/1520-0485(1982)012<0160:HEFOMA>2.0.CO;2.

Oort, A., S. Ascher, S. Levitus, and J. Peixóto, 1989: New estimates of the available potential energy in the World Ocean. *J. Geophys. Res.,* **94,** 3187–3200, doi:10.1029/JC094iC03p03187.

——, L. Anderson, and J. Peixóto, 1994: Estimates of the energy cycle of the oceans. *J. Geophys. Res.,* **99,** 7665–7688, doi:10.1029/93JC03556.

Panetta, R. L., 1993: Zonal jets in wide baroclinically unstable regions: Persistence and scale selection. *J. Atmos. Sci.,* **50,** 2073–2106, doi:10.1175/1520-0469(1993)050<2073:ZJIWBU>2.0.CO;2.

Pedlosky, J., 1987: *Geophysical Fluid Dynamics.* Springer-Verlag, 710 pp.

Plumb, R. A., and R. Ferrari, 2005: Transformed Eulerian-mean theory. Part I: Nonquasigeostrophic theory for eddies on a zonal-mean flow. *J. Phys. Oceanogr.,* **35,** 165–174, doi:10.1175/JPO-2669.1.

Robinson, A. R., and J. C. McWilliams, 1974: The baroclinic instability of the open ocean. *J. Phys. Oceanogr.,* **4,** 281–294, doi:10.1175/1520-0485(1974)004<0281:TBIOTO>2.0.CO;2.

Roquet, F., C. Wunsch, and G. Madec, 2011: On the patterns of wind-power input to the ocean circulation. *J. Phys. Oceanogr.,* **41,** 2328–2342, doi:10.1175/JPO-D-11-024.1.

Salmon, R., 1978: Two-layer quasigeostrophic turbulence in a simple special case. *Geophys. Astrophys. Fluid Dyn.,* **10,** 25–52, doi:10.1080/03091927808242628.

Scott, R. B., and F. Wang, 2005: Direct evidence of an oceanic inverse kinetic energy cascade from satellite altimetry. *J. Phys. Oceanogr.,* **35,** 1650–1666, doi:10.1175/JPO2771.1.

——, and Y. Xu, 2009: An update on the wind power input to the surface geostrophic flow of the world ocean. *Deep-Sea Res. I,* **56,** 295–304, doi:10.1016/j.dsr.2008.09.010.

Sen, A., R. B. Scott, and B. K. Arbic, 2008: Global energy dissipation rate of deep-ocean low-frequency flows by quadratic bottom boundary layer drag: Computations from current-meter data. *Geophys. Res. Lett.,* **35,** L09606, doi:10.1029/2008GL033407.

Smith, K. S., 2007: The geography of linear baroclinic instability in Earth's oceans. *J. Mar. Res.,* **65,** 655–683, doi:10.1357/002224007783649484.

Smith, W. H., and D. T. Sandwell, 1997: Global sea floor topography from satellite altimetry and ship depth soundings. *Science,* **277,** 1956–1962, doi:10.1126/science.277.5334.1956.

Spall, M. A., 2000: Generation of strong mesoscale eddies by weak ocean gyres. *J. Mar. Res.,* **58,** 97–116, doi:10.1357/002224000321511214.

Tailleux, R., 2013: Available potential energy and exergy in stratified fluids. *Annu. Rev. Fluid Mech.,* **45,** 35–58, doi:10.1146/annurev-fluid-011212-140620.

Thompson, A. F., 2008: The atmospheric ocean: Eddies and jets in the Antarctic Circumpolar Current. *Philos. Trans. Roy. Soc. London,* **366,** 4529–4541, doi:10.1098/rsta.2008.0196.

——, 2010: Jet formation and evolution in baroclinic turbulence with simple topography. *J. Phys. Oceanogr.,* **40,** 257–278, doi:10.1175/2009JPO4218.1.

Tulloch, R., J. Marshall, C. Hill, and K. S. Smith, 2011: Scales, growth rates, and spectral fluxes of baroclinic instability in the ocean. *J. Phys. Oceanogr.,* **41,** 1057–1076, doi:10.1175/2011JPO4404.1.

Vallis, G. K., 2006: *Atmospheric and Oceanic Fluid Dynamics.* Cambridge University Press, 745 pp.

Venaille, A., G. K. Vallis, and K. S. Smith, 2011: Baroclinic turbulence in the ocean: Analysis with primitive equation and quasigeostrophic simulations. *J. Phys. Oceanogr.,* **41,** 1605–1623, doi:10.1175/JPO-D-10-05021.1.

Volkov, D. L., and L.-L. Fu, 2008: The role of vorticity fluxes in the dynamics of the Zapiola anticyclone. *J. Geophys. Res.,* **113,** C11015, doi:10.1029/2008JC004841.

——, T. Lee, and L.-L. Fu, 2008: Eddy-induced meridional heat transport in the ocean. *Geophys. Res. Lett.,* **35,** L20601, doi:10.1029/2008GL035490.

von Storch, J. S., C. Eden, I. Fast, H. Haak, D. Hernández-Deckers, E. Maier-Reimer, J. Marotzke, and D. Stammer, 2012: An estimate of the Lorenz energy cycle for the world ocean based on the 1/10° STORM/NCEP simulation. *J. Phys. Oceanogr.,* **42,** 2185–2205, doi:10.1175/JPO-D-12-079.1.

Waterman, S. N., and S. R. Jayne, 2011: Eddy-mean flow interactions in the along-stream development of a western

boundary current jet: An idealized model study. *J. Phys. Oceanogr.,* **41,** 682–707, doi:10.1175/2010JPO4477.1.

Whitehead, J., 1975: Mean flow generated by circulation on a β-plane: An analogy with the moving flame experiment. *Tellus,* **27,** 358–364, doi:10.1111/j.2153-3490.1975.tb01686.x.

Wilkin, J. L., and R. A. Morrow, 1994: Eddy kinetic energy and momentum flux in the Southern Ocean: Comparison of a global eddy-resolving model with altimeter, drifter, and current-meter data. *J. Geophys. Res.,* **99,** 7903–7916, doi:10.1029/93JC03505.

Williams, R. G., C. Wilson, and C. W. Hughes, 2007: Ocean and atmosphere storm tracks: The role of eddy vorticity forcing. *J. Phys. Oceanogr.,* **37,** 2267–2289, doi:10.1175/JPO3120.1.

Witter, D. L., and D. B. Chelton, 1998: Eddy–mean flow interaction in zonal oceanic jet flow along zonal ridge topography. *J. Phys. Oceanogr.,* **28,** 2019–2039, doi:10.1175/1520-0485(1998)028<2019:EMFIIZ>2.0.CO;2.

Wortham, C., 2013: A multi-dimensional spectral description of ocean variability with applications. Ph.D. thesis, Massachusetts Institute of Technology and Woods Hole Oceanographic Institution, 184 pp.

——, and C. Wunsch, 2014: A multidimensional spectral description of ocean variability. *J. Phys. Oceanogr.,* **44,** 944–966, doi:10.1175/JPO-D-13-0113.1.

Wunsch, C., 1998: The work done by the wind on the oceanic general circulation. *J. Phys. Oceanogr.,* **28,** 2332–2340, doi:10.1175/1520-0485(1998)028<2332:TWDBTW>2.0.CO;2.

——, and R. Ferrari, 2004: Vertical mixing, energy, and the general circulation of the oceans. *Annu. Rev. Fluid Mech.,* **36,** 281–314, doi:10.1146/annurev.fluid.36.050802.122121.

——, P. Heimbach, R. Ponte, I. Fukumori, and ECCO-Consortium members, 2009: The global general circulation of the ocean estimated by the ECCO-Consortium. *Oceanography,* **22,** 88–103, doi:10.5670/oceanog.2009.41.

Zhai, X., and D. P. Marshall, 2013: Vertical eddy energy fluxes in the North Atlantic subtropical and subpolar gyres. *J. Phys. Oceanogr.,* **43,** 95–103, doi:10.1175/JPO-D-12-021.1.

——, H. L. Johnson, D. P. Marshall, and C. Wunsch, 2012: On the wind power input to the ocean general circulation. *J. Phys. Oceanogr.,* **42,** 1357–1365, doi:10.1175/JPO-D-12-09.1.